TASK QUARTERLY 14 No 3, 209–225

ROTOR BLADE GEOMETRY OPTIMIZATION IN KAPLAN TURBINE

MARZENA BANASZEK AND KRZYSZTOF TESCH

Turbomachinery and Fluid Mechanics Department,
Gdansk University of Technology,
Narutowicza 11/12, 80-233 Gdansk, Poland
banaszek@mech.pg.gda.pl

(Received 23 August 2010; revised manuscript received 14 September 2010)

Abstract: This paper presents a description of the method and results of rotor blade shape optimization. The rotor blading constitutes a part of a turbine's flow path.

The optimization consists in selecting a shape that minimizes the polytrophic loss ratio [1]. The shape of the blade is defined by the mean camber line and thickness of the airfoil. The thickness is distributed around the camber line based on the ratio of distribution. A global optimization was done by means of Genetic Algorithms (GA) with the help of Artificial Neural Networks (ANN) for approximations. For the numerical simulation of a flow through the model Kaplan turbine, the geometry employed in the model was based on the actual geometry of the existing test stage. The fluid parameters and the boundary conditions for the model were based on experimental measurements which were carried out at the test stand at the Department of Turbomachinery and Fluid Mechanics at the Gdansk University of Technology. The shape of the blading was optimized for the operational point with a maximum efficiency.

Keywords: fluid mechanics, turbomachinery, genetic algorithms, artificial neural networks

Notation

$\boldsymbol{D}$ – deformation rate tensor,
f – airfoil centerline,
$\vec{g}$ – acceleration of gravity,
h – enthalpy,
k – kinetic energy of velocity fluctuations,
$\dot{m}$ – mass flow rate,
N_d – dissipated power,
p, p_e – hydrodynamic and effective pressure,
$\vec{r}$ – radius,
S – surface,
t – time,
T – temperature,
$\vec{U}$ – absolute velocity,
V – volume,

$\vec{W}$ – relative velocity,
∂ – boundary,
δ – thickness distribution coefficient,
Δ – thickness,
ε – dissipation of kinetic energy of velocity fluctuations,
ζ – loss coeficient,
η_p – polytropic efficiency,
κ – isentropic exponent,
λ, λ_t – molecular and turbulent conductive heat transfer coefficient,
μ, μ_t, μ_e – dynamic, turbulent, effective viscosity,
ρ – density,
τ_t – turbulence intensity,
ϕ_μ – dissipation function,
$\vec{\omega}$ – angular velocity,
$\underline{\boldsymbol{\Omega}}$ – spin tensor,
$\overline{(\cdot)}$ – area-based mean,
$\langle\cdot\rangle$ – time-based mean,
$(\cdot)'$ – fluctuation,
$(\cdot)^T$ – transposition.

1. Theory

1.1. Loss coefficient

The loss coefficient is defined on the basis of the enthalpy equation, given in the differential form [2]:

$$\rho\frac{\mathrm{dh}}{\mathrm{dt}} = \phi_\mu + \nabla\cdot(\lambda\nabla T) + \frac{\mathrm{dp}}{\mathrm{dt}} \tag{1}$$

Assuming there is no heat transfer, a transformation of Equation (1) makes it possible to define the polytropic efficiency as [1]:

$$\eta_p := \frac{h_1 - h_2}{-\int\limits_{p_1}^{p_2}\rho^{-1}\,\mathrm{d}p} = 1 - \frac{\int\limits_{t_1}^{t_2}\rho^{-1}\phi_\mu\,\mathrm{d}t}{-\int\limits_{p_1}^{p_2}\rho^{-1}\,\mathrm{d}p} \tag{2}$$

Thus, the desired loss coefficient definition may be expressed as:

$$\zeta := 1 - \eta_p = \frac{\int\limits_{t_1}^{t_2}\rho^{-1}\phi_\mu\,\mathrm{d}t}{-\int\limits_{p_1}^{p_2}\rho^{-1}\,\mathrm{d}p} \tag{3}$$

In the case of turbomachinery, an averaged coefficient of polytropic losses is introduced. The mean value is defined with respect to area-based averages of quantities found in definition (3). Thus, on the surface S we obtain [1]:

$$\bar{\zeta} := \frac{\iint\limits_S\int\limits_{t_1}^{t_2}\rho^{-1}\phi_\mu\,\mathrm{d}t\,\mathrm{d}S}{-\iint\limits_S\int\limits_{p_1}^{p_2}\rho^{-1}\,\mathrm{d}p\,\mathrm{d}S} \tag{4}$$

Replacing dt in the denominator with $\frac{\mathrm{d}L}{U}$ and utilising the formula for mass flow rate $\dot{m} = \rho S \bar{U}$, the definition (4) may be written in the following form for the control volume V contained between the inlet S_1 and the outlet S_2:

$$\bar{\zeta} = \frac{\rho}{\dot{m}} \frac{\iiint_V \phi_\mu \,\mathrm{d}V}{\bar{p}_1 - \bar{p}_2} \tag{5}$$

In the above equation, the mean pressure $\bar{p}$ is defined as an area-based average: $\bar{p} := S^{-1} \iint_S p \,\mathrm{d}S$. The denominator in Equation (5) is the power of mechanical energy dissipation N_d, computed for a known velocity field according to the formula [2]:

$$N_d := \iiint_V \phi_\mu \,\mathrm{d}V = 2\mu \iiint_V \boldsymbol{D}^2 \,\mathrm{d}V \tag{6}$$

The formula is valid for incompressible flows.

The formula (5) for the polytrope loss coefficient holds both for the laminar and the turbulent case. For turbulent flows, complete information about the velocity field is required; such may be obtained by employing the DNS solution scheme. On the other hand, if all we have is the averaged velocity field solution given by the RANS method, Equation (5) cannot be applied directly. For turbulent flows, the enthalpy Equation (1) takes on the following form upon averaging:

$$\rho \frac{\mathrm{d}\langle \mathrm{h} \rangle}{\mathrm{d}t} = 2\mu \langle \boldsymbol{D} \rangle^2 + \rho\varepsilon + \nabla \cdot ((\lambda + \kappa\lambda_t) \nabla \langle T \rangle) + \frac{\mathrm{d}\langle \mathrm{p} \rangle}{\mathrm{d}t} + \nabla \cdot \langle p' \vec{U}' \rangle \tag{7}$$

In the above expression three new terms have appeared, in comparison with Equation (1). They originate from averaging the nonlinear terms in Equation (1). The kinetic energy dissipation for velocity fluctuation ε results from averaging the dissipation function ϕ_μ and from the assumption of homogeneity. The turbulent heat flux $\lambda_t \nabla \langle T \rangle$ results from averaging the material derivative of temperature (by way of enthalpy). This relies on the additional hypothesis of turbulent diffusion [2]. The last term is the factor responsible for diffusion due to pressure and velocity fluctuations $\langle p' \vec{U}' \rangle$; it results from averaging the material derivative of pressure.

Let us again assume that there is no heat exchange through the molecular and turbulent mechanisms, thus, necessitating that $\langle T \rangle = const$. As in the equation for transport of kinetic energy of velocity fluctuations, it may be assumed that the diffusion due to pressure and velocity fluctuations is negligible $\langle p' \vec{U}' \rangle \approx \vec{0}$. The averaged enthalpy Equation (7) thus simplifies to the form:

$$\rho \frac{\mathrm{d}\langle \mathrm{h} \rangle}{\mathrm{d}t} = 2\mu \langle \boldsymbol{D} \rangle^2 + \rho\varepsilon + \frac{\mathrm{d}\langle \mathrm{p} \rangle}{\mathrm{d}t} \tag{8}$$

A comparison of (1) and (8) shows that they only differ by a single term, namely the turbulent dissipation. It cannot be neglected; for blade cascades this term is greater, by an order of magnitude, than the dissipation of mean flow [3, 4].

Following the same line of reasoning as above, it can be shown that the loss coefficient will take a form analogous to (5):

$$\langle\bar{\zeta}\rangle = \frac{\rho}{\dot{m}} \frac{\iiint_V \langle\phi_\mu\rangle \mathrm{d}V}{\langle\bar{p}_1\rangle - \langle\bar{p}_2\rangle} \tag{9}$$

where the averaged dissipation function is calculated as $\langle\phi_\mu\rangle = 2\mu\langle\boldsymbol{D}\rangle^2 + \rho\varepsilon$. The symbol $\langle\bar{p}\rangle$ is to be understood as the area-based average of pressure, obtained from a RANS solution.

1.2. Dissipation in a rotating system

In a rotating system of reference, the absolute velocity vector $\vec{U}$ decomposes into two components. The first component is the relative velocity $\vec{W}$ and the other is frame rotational velocity $\vec{\omega}\times\vec{r}$. This may be written as $\vec{U} = \vec{W} + \vec{\omega}\times\vec{r}$. This decomposition should be inserted into the definition of the deformation rate tensor [2] $\boldsymbol{D} := 2^{-1}(\nabla\vec{U} + (\nabla\vec{U})^T)$. Transforming this expression, we obtain:

$$\boldsymbol{D} = \boldsymbol{D}_W + 2^{-1}\left(\nabla(\vec{\omega}\times\vec{r}) + (\nabla(\vec{\omega}\times\vec{r}))^T\right) \tag{10}$$

where $\boldsymbol{D}_W$ is the deformation velocity tensor in the rotating frame of reference. The rotational velocity gradient is given by:

$$\nabla(\vec{\omega}\times\vec{r}) = \begin{pmatrix} 0 & \omega_z & -\omega_y \\ -\omega_z & 0 & \omega_x \\ \omega_y & -\omega_x & 0 \end{pmatrix} = \boldsymbol{\Omega}^T \tag{11}$$

which amounts to a transposition of the spin tensor $\boldsymbol{\Omega}$. It may similarly be shown that $(\nabla(\vec{\omega}\times\vec{r}))^T = \boldsymbol{\Omega}$. The Equation (10) may now be written as:

$$\boldsymbol{D} = \boldsymbol{D}_W + 2^{-1}\left(\boldsymbol{\Omega}^T + \boldsymbol{\Omega}\right) = \boldsymbol{D}_W \tag{12}$$

inasmuch as $\boldsymbol{\Omega}^T + \boldsymbol{\Omega} = \boldsymbol{0}$. This confirms the invariance of the dissipation function which is computed from tensor $\boldsymbol{D}$. The above analysis remains correct also if the angular velocity $\vec{\omega}$ changes over time. Furthermore, it remains correct for a compressible flow since, as can easily be verified, $\nabla\cdot\vec{U} = \nabla\cdot\vec{W}$. In cases where the dissipation function has been averaged, a new term appears related to turbulent dissipation. As turbulent dissipation is a scalar, it remains the same in both frames of reference.

1.3. System of equations

The closed system of equations for turbulent flows of incompressible fluids [2] consists of the averaged continuity Equation (13a), and the vector Reynolds Equation (13b). The form of additional equations depends on the turbulence model adopted. For the two-equation k-ε model, the Boussinesq assumption holds. The first of these equations is the equation for transport of kinetic energy of velocity fluctuations k, in the form (13c). The other is the equation for transport of dissipation of kinetic energy of velocity fluctuations ε, in the form (13d). Both equations contain the modelled terms. The last equation is the equation for

turbulent viscosity μ_t, in the form (13e). The system of seven (scalar) equations appears as follows:

$$\nabla \cdot \langle \vec{U} \rangle = 0 \tag{13a}$$

$$\rho \frac{\mathrm{d}\langle \vec{\mathrm{U}} \rangle}{\mathrm{dt}} = \rho \vec{g} - \nabla p_e + \nabla \cdot (2\mu_e \langle \boldsymbol{D} \rangle) \tag{13b}$$

$$\rho \frac{\mathrm{dk}}{\mathrm{dt}} = 2\mu_t \langle \boldsymbol{D} \rangle^2 + \nabla \cdot \left(\left(\mu_t \sigma_k^{-1} + \mu \right) \nabla k \right) - \rho\varepsilon \tag{13c}$$

$$\rho \frac{\mathrm{d}\varepsilon}{\mathrm{dt}} = C_{\varepsilon 1} k^{-1} \varepsilon 2\mu_t \langle \boldsymbol{D} \rangle^2 + \nabla \cdot \left(\left(\mu_t \sigma_\varepsilon^{-1} + \mu \right) \nabla \varepsilon \right) - C_{\varepsilon 2} \rho k^{-1} \varepsilon^2 \tag{13d}$$

$$\mu_t = C_\mu \rho k^2 \varepsilon^{-1} \tag{13e}$$

In the above, p_e denotes effective pressure $p_e := \langle p \rangle + \frac{2}{3}\rho k$, and μ_e denotes effective viscosity $\mu_e := \mu + \mu_t$. The system contains seven unknowns $\langle U_x \rangle$, $\langle U_y \rangle$, $\langle U_z \rangle$, $\langle p \rangle$, k, ε, μ_t, and thus constitutes a closed system as long as the constants C_μ, σ_k, σ_ε, $C_{\varepsilon 1}$, $C_{\varepsilon 2}$ are known.

1.4. Airfoil description

The profile is defined in terms of centerline (center surface) f and thickness function Δ distributed along the centerline [5–7]. The centerline is obtained as the arithmetic mean of the pressure- and suction-side profiles of the airfoil.

The thickness function may be distributed in various ways depending on the distribution coefficient δ (Figure 1). The coefficient may vary along the centerline or have a constant value. In either case it takes on values within the range of $[0;1]$.

This may be written as $\delta : \mathbb{R} \to [0;1]$ (on a 2D plane) or $\delta : \mathbb{R}^2 \to [0;1]$ (in 3D space). The pressure-side profile is obtained from $f - (1-\delta)\Delta$, and the suction-side profile from $f + \delta\Delta$. This holds for the planar case, as well as for the spatial case (in cylindrical coordinates, for instance). Within the scope of the current project, the coefficient δ has been held constant. The original, unoptimized airfoil results from setting $\delta = \frac{1}{2}$ (Figure 2). For thickness distribution coefficient $\delta = 0$, the centerline coincides with the suction-side profile, while for $\delta = 1$ the centerline coincides with the pressure-side of the airfoil. In general, there is no reason why $\delta = 0$ should not exceed 1 or drop below 0. However, if this is allowed, the centerline will no longer be contained within the boundaries of the airfoil profile.

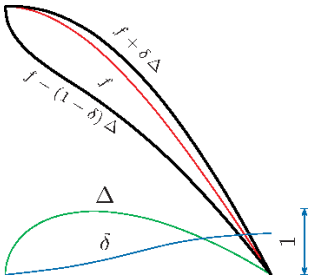

Figure 1. Airfoil geometry

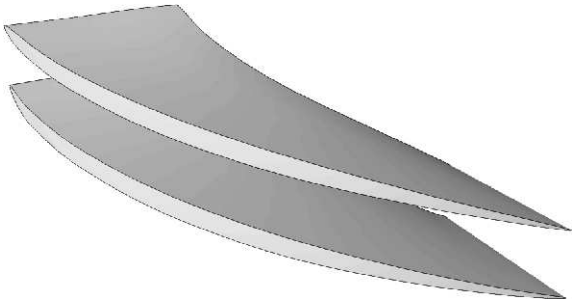

Figure 2. Rotor blades for $\delta = \frac{1}{2}$ (top) and $\delta = 0$ (bottom)

2. CFD

2.1. Flow configuration

Figure 3 shows the model hydraulic turbine configuration. Within the scope of the current work, the investigated region has been bounded within transverse planes 0 and 3 (Figure 4). As a result, the draft tube, located below plane 3, is not accounted for in the investigation. A uniform inflow at plane 0 has been assumed. Plane 1 divides the preliminary stator (6 vanes) from the stator ring proper (12 vanes). Plane 2 divides the stator from the rotating rotor.

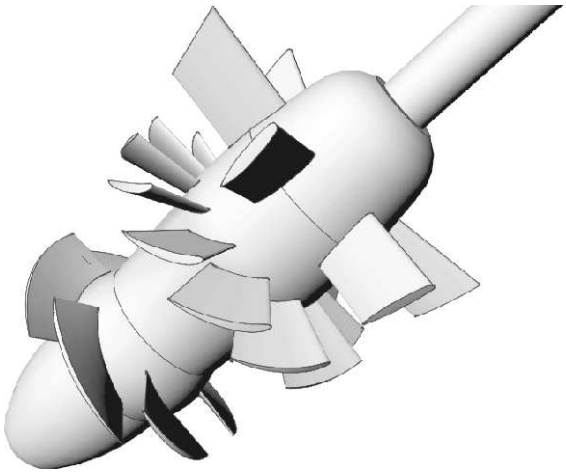

Figure 3. Flow configuration of model turbine

Owing to the sixfold symmetry of the geometry, only a section has been modeled, as shown in Figure 5. The computational volume is divided into three regions. The first region encompasses the pre-stator, incorporating one of its blades. The second region includes two blades of the stator proper (which has twelve blades altogether, so that two fit in a sixth section). This match between the two stator sections obviates the need for scaling the interface between successive regions, which otherwise could introduce additional errors in the CFD solutions. The third region includes one of the six rotor blades, and rotates with respect

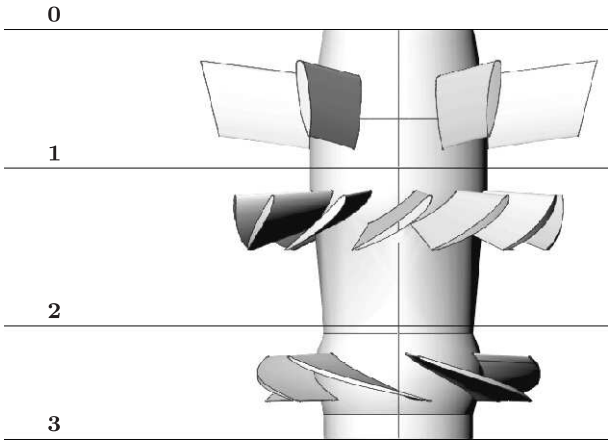

Figure 4. Part of flow configuration with dividing planes marked

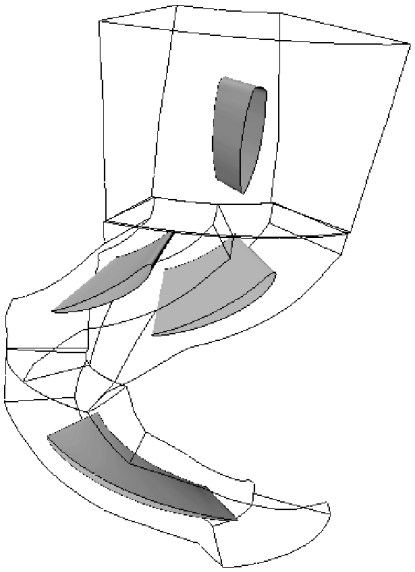

Figure 5. $\frac{1}{6}$ sector of flow volume

to the stator regions with an angular velocity of 650RPM. One of the region's bounding surfaces (the outer casing of the duct) is set stationary within the absolute frame.

2.2. Principal boundary conditions

The principal boundary conditions include:

- Inlet: The mass flow rate is $\dot{m} = 74\text{kg/s}$, normal to plane 0 in Figure 4. The arbitrarily adopted k-ε turbulence model called for additional parameters k i ε to be set. A typical level of turbulence at inlet corresponding to turbulence intensity $\tau_t = 5\%$ and ratio of turbulent to molecular viscosity

$\mu_t/\mu = 10$ has been assumed. The parameters k i ε at inlet may be computed on the basis of τ_t i μ_t/μ using the formulas [2] $k = 3\langle U\rangle^2\tau_t 2^{-1}$, $\varepsilon = c_\mu \rho k^2 \mu_t^{-1}$.

- Outlet: Due to the strong variability of velocity at the outlet plane (plane 3 in Figure 4) it would be ill-advised to set a constant pressure distribution there. An arbitrarily constant pressure would impose nonphysical changes on the velocity field. For that reason it has been decided to set a boundary condition in the form of a mass flow rate matching the inlet flow rate.
- Walls: The walls have been set as impermeable and non-slip, forcing $\langle\vec{U}\rangle = \vec{0}$. Naturally for the rotating walls of the rotor assembly, the corresponding velocity is set as $\langle\vec{U}\rangle = \vec{\omega}\times\vec{r}$.
- Periodicity: The periodic boundary conditions over 60° rotation were set on boundaries resulting from taking a $(\frac{1}{6})$ section of the flow volume.
- Interfaces: There are two kinds of interfaces. The first is a *fluid-fluid* interface between the pre-stator region and the stator region, at plane 1. This has been necessary, as the meshing on plane 1 on the pre-stator side does not match the arrangement of the 1 plane on the stator side. The other interface of type *stator-frozen rotor* is located at the 2 plane to account for proper interaction between the stationary mesh on the stator side and the rotating mesh on the rotor side.

The flow has been modeled as stationary. The interaction between the stator and the rotor has been modeled as of the *stator-frozen rotor* type. This means that the rotor is considered in a fixed position (but not zero velocity) with respect to the stator. This may be justified under the circumstances, considering that there is an unusually large gap between the stator and the rotor (necessary to introduce measuring probes into the model turbine). Also, a stationary simulation is significantly quicker than a transient one, an important factor when the large number of runs needed for adequate optimization is considered.

2.3. Mesh

The individual computational regions were meshed with hexahedral elements. The mesh statistics for the entire volume is given in Table 1. A meshed rotor blade for thickness distribution coefficient $\delta = \frac{1}{2}$ is shown in Figure 6. The rotor meshes included a gap between rotor and duct wall, set at 2.5% of the radial distance between the hub and the outer wall.

Table 1. Mesh statistics

	$\delta = 0$	$\delta = \frac{1}{2}$
Nodes	764541	790941
Elements	712656	738256

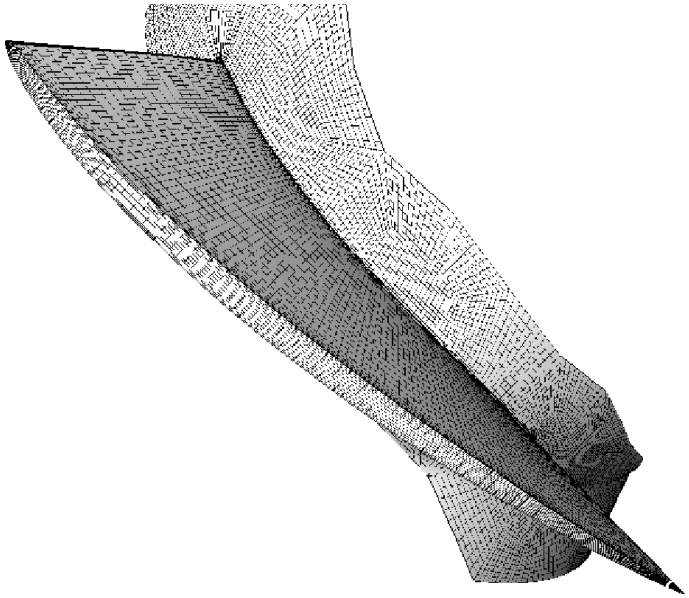

Figure 6. Rotor mesh for $\delta = \frac{1}{2}$

3. Optimization

3.1. Approximation with neural nets

To reduce the CFD computational requirements, a neural net has been employed to approximate loss coefficient ζ for varying thickness distribution coefficients δ. The structure of the net is shown in Figure 7. It is an unidirectional, two-layer net [8] with 13 weights. The first layer contains 4 neurons. As befits its purpose, the net has a single input δ and single output ζ. The net was trained using the method of error backpropagation over a small run of training data. The training data are shown as dots on the plot in Figure 8. The learning error did not exceed $2 \cdot 10^{-5}$.

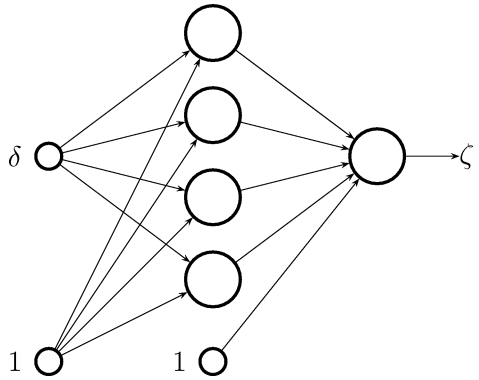

Figure 7. Neural net structure

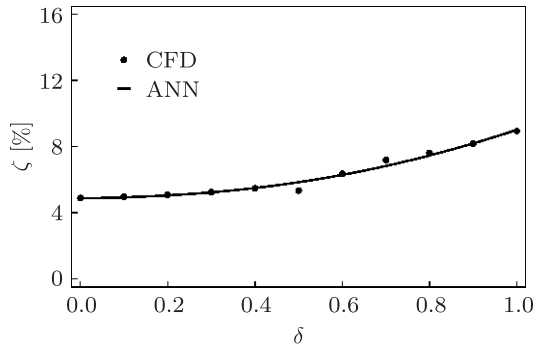

Figure 8. Distribution of ζ as a function of δ according to CFD and ANN

Table 2. GA parameters and statistics

	Value
Chromosome length	1
Population size	30
Tournament size	3
Crossover probability	0.7
Mutation probability	0.15
Variable range	[0;1]
Generation count	20
Crossover count	203
Mutation count	89

Figure 8 shows a comparison between the ζ values obtained from CFD simulation and given by the neural net, for thickness distribution coefficient $\delta \in [0;1]$. There is sufficient agreement between computation and approximation.

3.2. Optimization with genetic algorithms

The trained neural net was used to compute the target function values during optimization by means of genetic algorithms, employing the AGA program [9]. The program uses floating point representations of chromosomes [10]. Table 2 summarizes the basic data and statistics for the GA. As there is only one

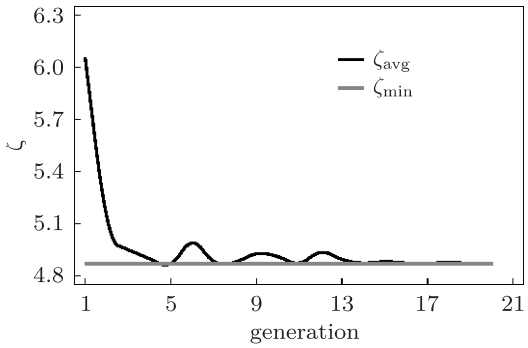

Figure 9. GA convergence

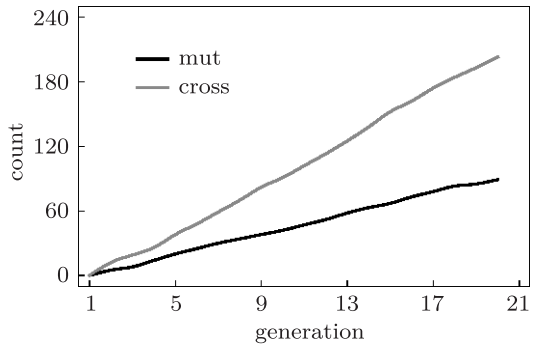

Figure 10. GA mutation and crossovers count

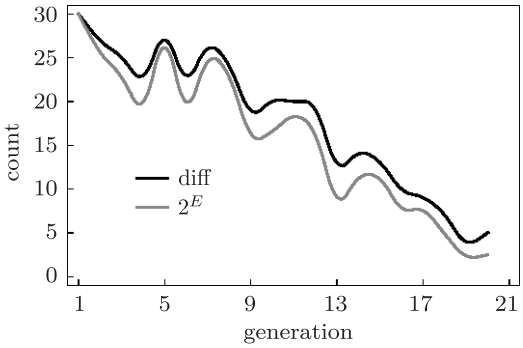

Figure 11. GA entropy and number of distinct individuals

independent variable and the representation is of the floating-point type, the chromosome length is 1. The population size was taken as 30, which seemed sufficient for a single variable optimization. Ditto for the number of generations, taken as 20. Convergence is readily achieved in several generations.

Figure 9 shows the GA convergence. The symbol ζ_{avg} denotes the mean loss coefficient for the entire population, while ζ_{min} is the global minimum for the entire optimization process. The optimum is obtained for $\delta \approx 0$.

Figure 10 shows how the mutation count (mut) and the crossovers count (cross) change during the optimization process for the probabilities taken from Table 2. Figure 11 shows the number of distinct individuals for each generation (diff) and the corresponding 2^E factor, where E is entropy in the statistical sense. These figures make it possible to monitor the population variability. Another population variability indicator is discrepancy [11]. The discrepancy plot (D) is shown in Figure 12. Discrepancy takes on values in the neighborhood of 0 for random populations and close to 1 for uniform populations.

4. Results

4.1. Loss coefficients

Table 3 shows an example of computational results for a CFD run. Indexes 0–3 correspond to the cross-sectional planes as shown in Figure 4. The quantity

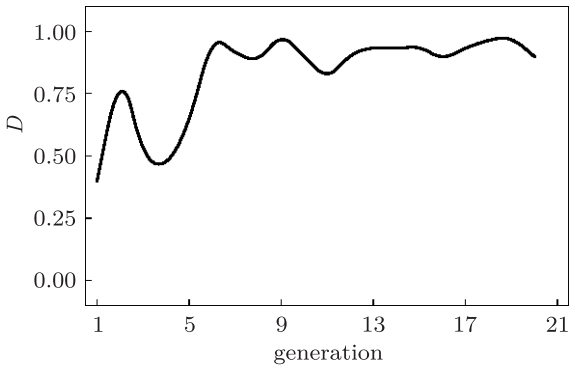

Figure 12. GA discrepancy D

$N_{da} = \iiint_V 2\mu\langle \boldsymbol{D}\rangle^2 \,\mathrm{d}V$ corresponds to the dissipative power in the mean flow, while $N_{dt} = \iiint_V \rho\varepsilon \,\mathrm{d}V$ is the dissipative power of turbulence. The total dissipative power is computed as $N_d = \iiint_V \langle\phi_\mu\rangle \,\mathrm{d}V = N_{da} + N_{dt}$. Subscript p denotes the pre-stator, s the stator proper, and r the rotor. Loss coefficient ζ is computed for the entire flow volume.

Table 3. Sample results

	$\delta = 0$	$\delta = \frac{1}{2}$
p_0 [kPa]	27.201	22.669
p_1 [kPa]	26.639	22.106
p_2 [kPa]	18.425	13.878
p_3 [kPa]	−0.337	−0.026
$N_{da,p}$ [W]	0.038	0.038
$N_{da,s}$ [W]	0.723	0.722
$N_{da,w}$ [W]	1.685	1.480
N_{da} [W]	2.447	2.240
$N_{dt,p}$ [W]	0.600	0.600
$N_{dt,s}$ [W]	22.000	22.080
$N_{dt,r}$ [W]	74.974	64.813
N_{dt} [W]	97.575	87.493
N_d [W]	100.021	89.733
ζ_p [%]	1.532	1.531
ζ_s [%]	3.731	3.737
ζ_r [%]	5.510	6.430
ζ [%]	4.898	5.332

Figure 13 shows the loss coefficient distribution as a function of the thickness coefficient.

4.2. Pressure distribution

Figure 14 shows dimensionless pressure drops on the pre-stator, the stator, the rotor, and overall. A dimensionless drop means the ratio of the actual pressure drop value to the value obtained for the original configuration (with $\delta = \frac{1}{2}$) for the entire flow volume. Under this definition, the point $(\frac{1}{2},1)$ denotes the overall

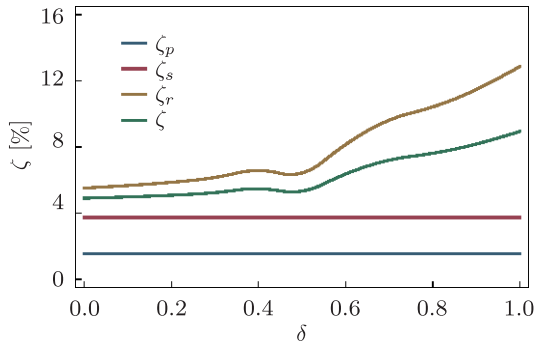

Figure 13. Distribution of ζ as function of δ

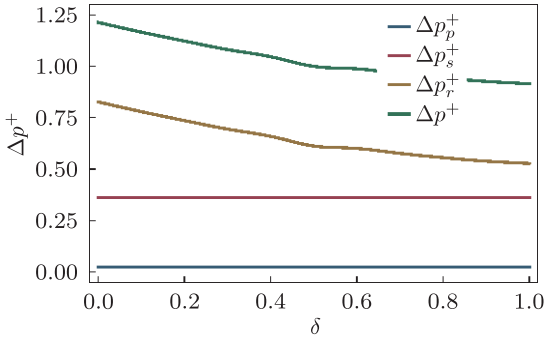

Figure 14. Δp^+ distribution as function of δ

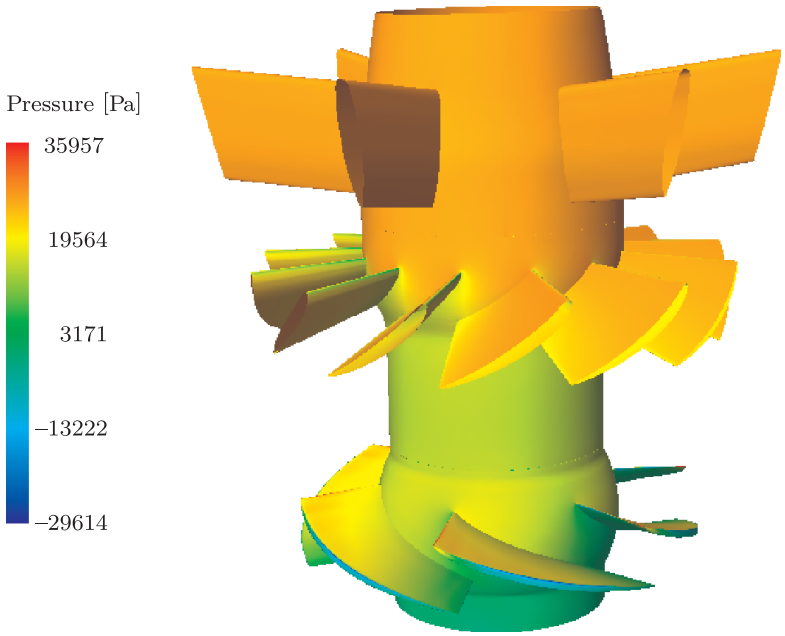

Figure 15. Distribution of p over the turbine for $\delta = 0$

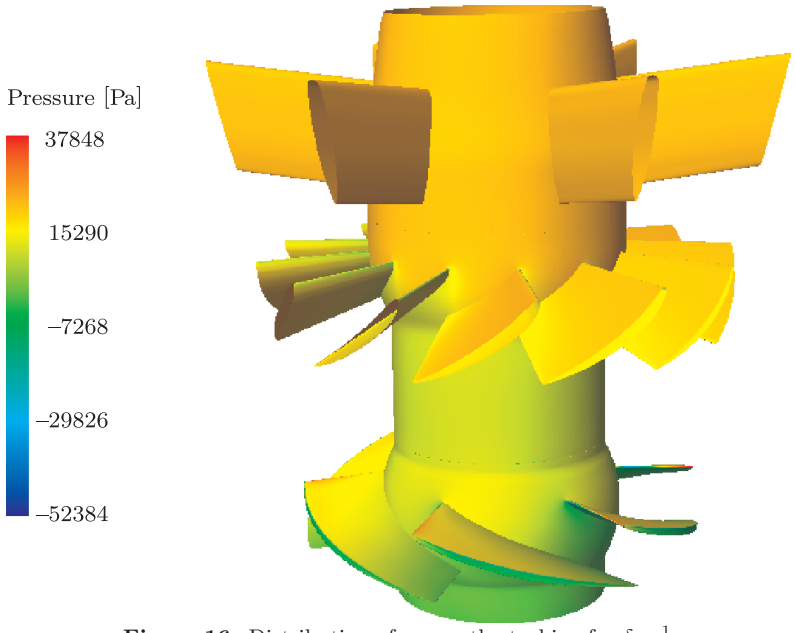

Figure 16. Distribution of p over the turbine for $\delta = \frac{1}{2}$

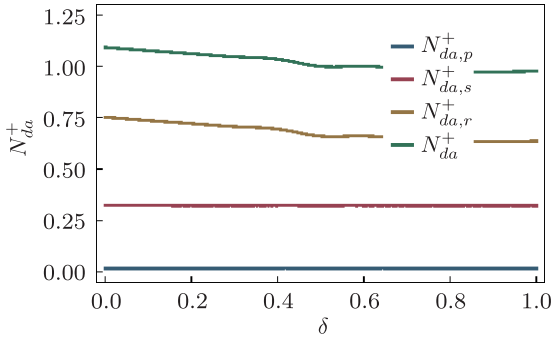

Figure 17. N^+_{da} distribution as function of δ

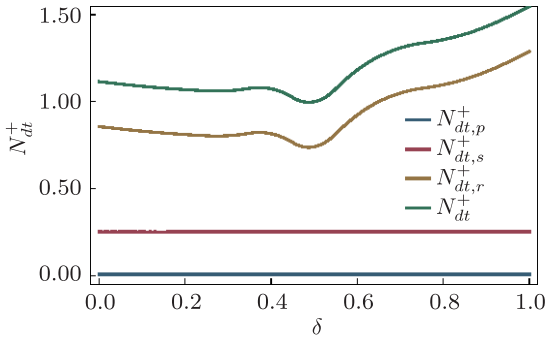

Figure 18. N^+_{dt} distribution as function of δ

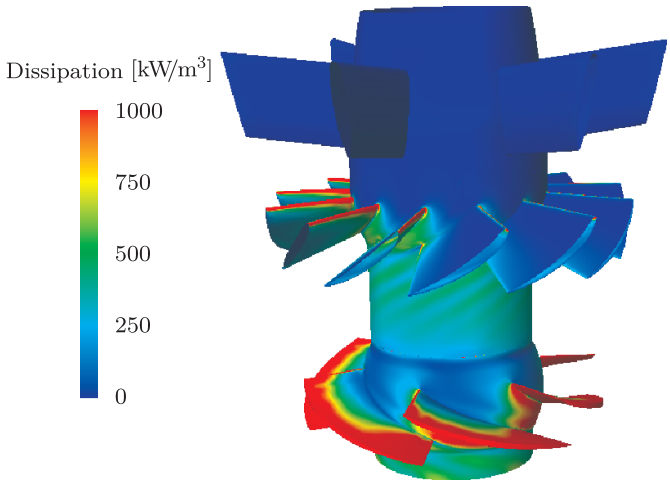

Figure 19. Distribution of $\langle \phi_\mu \rangle$ over the turbine for $\delta = 0$

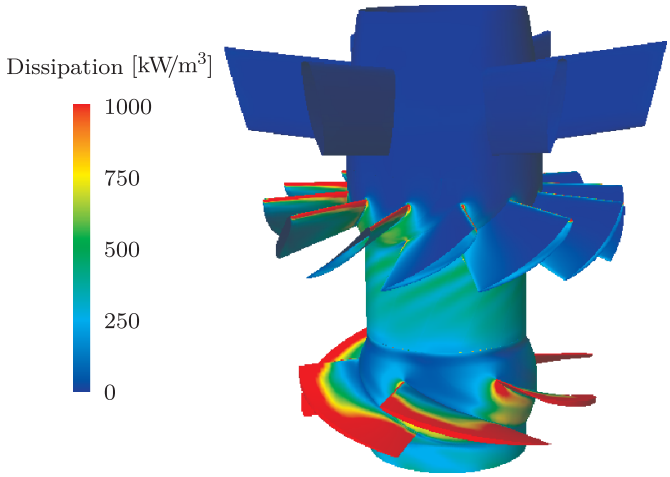

Figure 20. Distribution of $\langle \phi_\mu \rangle$ over the turbine for $\delta = \frac{1}{2}$

pressure drop for $\delta = \frac{1}{2}$. It may be observed that for falling δ the pressure drop increases. The changes occur principally in the rotor region, governing the overall trend. Changes at the stator are negligible.

Figures 15 and 16 show the distribution of hydrodynamic gauge pressures over turbine surfaces.

4.3. Dissipation intensity

Figure 17 shows the dimensionless dissipated power of the mean flow, while Figure 18 shows the dimensionless dissipated power of turbulent fluctuations over the pre-stator, stator, rotor, and overall. The dimensionless dissipated power is defined as the ratio of the actual dissipated power to the dissipated power obtained for the original configuration (with $\delta = \frac{1}{2}$) for the entire flow volume.

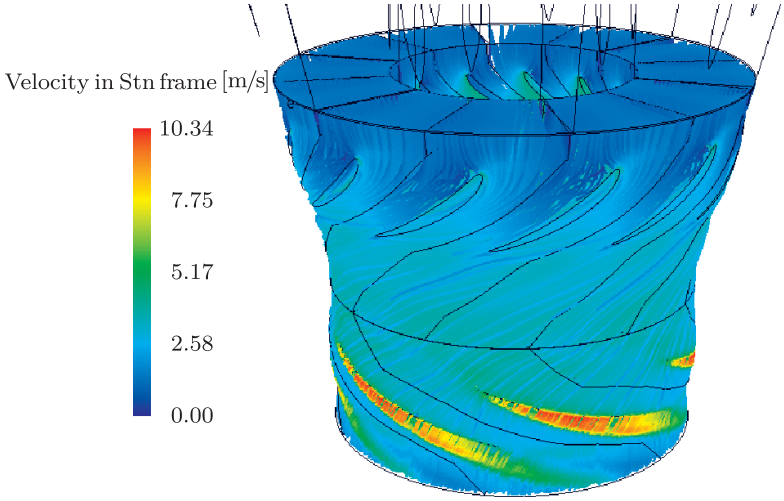

Figure 21. Streamlines for $\delta = 0$

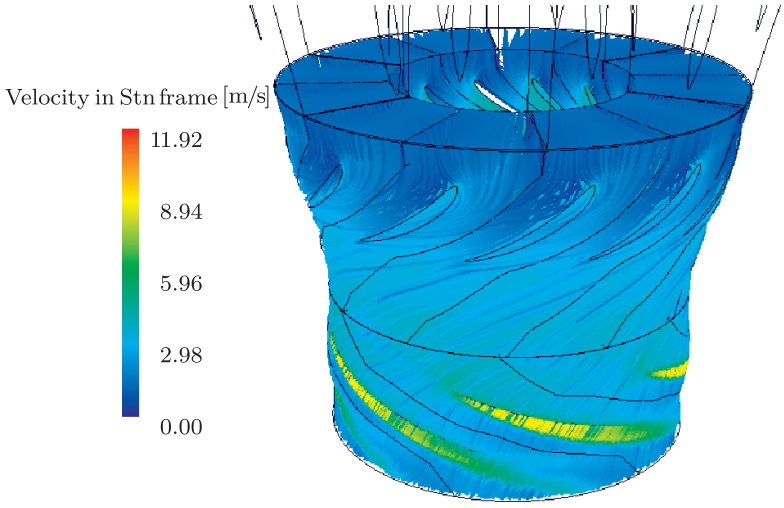

Figure 22. Streamlines for $\delta = \frac{1}{2}$

The point $(\frac{1}{2},1)$ denotes the overall dissipated power for $\delta = \frac{1}{2}$. The dissipation in the mean flow increases in an inverse manner with δ. The dissipation in turbulent fluctuations has local maxima and minima dependent on δ. Table 3 also indicates that N_{dt} is larger by at least an order of magnitude than N_{da} [3, 4].

Figures 19 and 20 show the distribution of $\langle \phi_\mu \rangle$ over the turbine. The graph scale has been truncated on the upper bound for both plots.

4.4. Streamlines

Figures 21 and 22 show streamlines in an absolute frame of reference for both values of δ. Streamlines are traced for the stator proper (w/o pre-stator)

and the rotor. It may be observed that rotor blades extract most of the angular momentum generated by the stator.

5. Conclusions

- The airfoil minimizing loss coefficient ζ is obtained for thickness distribution coefficient $\delta = 0$. This means that the airfoil is more curved with respect to the original blade at $\delta = \frac{1}{2}$.
- More power is dissipated with lower values of δ, but the pressure drop increases as well, which causes the overall loss coefficient to decrease.
- The optimizing calculations indicate that by merely changing a constant thickness coefficient for the rotor, the loss coefficient ζ may be reduced by about 1.4, for the flow configuration in question.
- It is possible to further reduce coefficient ζ by adjusting the shape of the stator vane along with changes in the rotor blade.
- The loss coefficients for the individual regions of the flow volume (*i.e.* the stator, rotor, *etc.*) do not add up. Higher values of ζ were obtained for the rotor. It must be remembered, however, that the computation did not include the flow in the draft tube.

References

[1] Puzyrewski R 1992 *Fundamentals of Turbomachinery Theory - One Dimensional Approach*, Ossolineum, Wroclaw, Poland (in Polish)
[2] Tesch K 2008 *Fluid Mechanics*, Gdansk University of Technology Publishing, Gdansk (in Polish)
[3] Tesch K 1999 *Report of IMP PAN 630/99*, Gdansk, Poland (in Polish)
[4] Tesch K 2000 *Scientific Issue IMP PAN 516/1475*, Gdansk, Poland (in Polish)
[5] Puzyrewski R 1997 *Report of IMP PAN 256/97*, Gdansk, Poland (in Polish)
[6] Tesch K 1999 *Report of IMP PAN 388/99*, Gdansk, Poland (in Polish)
[7] Tesch K 2002 *Two Dimensional Blade Shape Optimisation by Means of Genetic Algorithms*, *15th National Conf. on Fluid Mechanics*, Augustow, Poland (on CD) (in Polish)
[8] Osowski S 1996 *Artificial Neural Network - An Algorithmic Approach*, WNT, Warsaw, Poland (in Polish)
[9] *http://www.pg.gda.pl/∼krzyte/ga/ga.html*
[10] Michalewicz Z 1996 *Genetic Algorithms + Data Structures = Evolution Programs*, Springer
[11] Thiémard E 2001 *J. Complexity* **17** (4) 850